Available online at www.sciencedirect.com
ScienceDirect
Journal of Hazardous Materials 159 (2008) 235–244
Journal of Hazardous Materials
www.elsevier.com/locate/jhazmat

Removal of copper ions by modified Unye clay, Turkey

Erdal Eren *

Ahi Evran University, Faculty of Arts and Sciences, Department of Chemistry, 40100 Kirsehir, Turkey

Received 15 November 2007; received in revised form 6 February 2008; accepted 7 February 2008
Available online 17 February 2008

Abstract

This paper presents the adsorption of Cu(II) from aqueous solution on modified Unye bentonite. Adsorption of Cu(II) by manganase oxide modified bentonite (MMB) sample was investigated as a function of the initial Cu(II) concentration, solution pH, ionic strength, temperature and inorganic ligands (Cl^-, SO_4^{2-}, HPO_4^{2-}). Changes in the surfaces and structure were characterized using X-ray diffraction (XRD), infrared (IR) spectroscopy, N_2 gas adsorption and potentiometric titration data. The adsorption properties of raw bentonite (RB) were further improved by modification with manganese oxide. Langmuir monolayer adsorption capacity of the MMB (105.38 mg/g) was found greater than that of the raw bentonite (42.41 mg/g). The spontaneity of the adsorption process is established by decrease in ΔG which varied from −4.68 to −5.10 kJ mol^{-1} in temperature range 303–313 K. The high performance exhibited by MMB was attributed to increased surface area and higher negative surface charge after modification.

Keywords: Bentonite; Adsorption; Thermodynamic; Heavy metal; Copper

1. Introduction

Heavy metal pollution occurs in many industrial wastewater such as those produced by metal plating facilities, mining operations, battery manufacturing process, the production of paints and pigments, and the glass production industry. Although a limit of 2 mg/L was proposed by the World Health Organization as the provisional guideline value for copper content of drinking water, intake of excessively large doses of copper by man leads to severe mucosal irritation and corrosion, widespread capillary damage, hepatic and renal damage and central nervous system irritation followed by depression. Severe gastrointestinal irritation and possible necrotic changes in the liver and kidney could occur [1].

Conventional technologies for the removal of heavy metal such as chemical precipitation, electrolysis, ion exchange and reverse osmosis are often neither effective nor economical [2,3]. Among the physico-chemical treatment process adsorption is highly effective, cheap and easy to adapt [4]. Adsorption has been proven to be a successful method for removal of heavy metals from wastewater. Activated carbon is highly effective in adsorbing heavy metals from wastewater but high cost limits its use [5,6]. The abundance of clay minerals and their low cost are a strong candidate as an adsorbent for removal of heavy metal from wastewater.

Any clay of volcanic origin that contains montmorillonite is referred to as bentonite. It belongs to the 2:1 clay family, the basic structural unit of which is composed of two tetrahedrally coordinated sheets of silicon ions surrounding a sandwiched octahedrally coordinated sheet of aluminum ions [7]. Compared with other clay types, it has excellent adsorption properties and possesses adsorption sites available within its interlayer space as well as on the outer surface and edges [8–10]. Infrared (IR) spectroscopy has significantly contributed to the understanding of the structure, bonding, and reactivity of clay minerals [11–17].

Solid separation and sludge management after the metal adsorption on oxides is difficult, because the oxides are usually in colloidal forms. One possible solution to this problem is to prepare a modified adsorbent that can be used in an adsorption process. Modified adsorbents of this type include manganese oxide coated zeolite [18], manganese oxide coated sand [19], and iron oxide coated clay [20,21].

A composite adsorbent, manganese oxide coated bentonite (MMB), was proposed and studied in this research. The reason for choosing manganese oxides is that relative to Fe or Al oxides, manganese oxides have a higher affinity for many heavy

* Tel.: +90 362 312 19 19; fax: +90 362 457 60 80.
E-mail address: erdalern@omu.edu.tr.

0304-3894/$ – see front matter © 2008 Elsevier B.V. All rights reserved.
doi:10.1016/j.jhazmat.2008.02.035

Nomenclature

C_e	equilibrium concentration of the adsorbate in the solution (mg/L)
K_F	Freundlich constant indicative of the adsorption capacity of the adsorbent (mg/g)
K_L	constant that represents the energy or net enthalpy of adsorption (L/mg)
m	mass of adsorbent (g/L)
MMB	manganese oxide modified bentonite
n	experimental constant indicative of the adsorption intensity of the adsorbent
q_e	amount of adsorbate removed from aqueous solution at equilibrium (mg/g)
q_m	mass of adsorbed solute completely required to saturate a unit mass of adsorbent (mg/g)
RB	raw bentonite

metals [22]. In fact, several investigators have suggested applications for manganese oxides in water and wastewater treatment [22–25]. Bentonite, which has a high surface area, should provide an efficient surface for the manganese oxide. At the same time, the manganese oxides can improve the metal adsorption capacity of bentonite. MMB was examined in batch experiments for the removal of Cu(II) from aqueous solution (i.e. simulated wastewaters) in order to examine whether this separation technique may improve bentonite performance as a Cu(II) adsorbent. The influence of pH, ionic strength, ligands (Cl^-, SO_4^{2-}, HPO_4^{2-}) and temperature on the adsorption of Cu(II) by the RB and MMB samples was investigated to better understand the Cu(II) adsorption process.

2. Experimental

2.1. Materials

2.1.1. Preparation of RB

The bentonite sample (from Unye, Turkey) was grounded and washed in deionized water several times at a 1:10 bentonite/water ratio. The mixture was stirred for 3 h and then kept standing overnight, followed by separation, washing and drying at 60 °C. RB had a mineral composition of 76% montmorillonite, 8% quartz, 12% dolomite and 4% other minerals. RB was composed of 62.70% SiO_2, 20.10% Al_2O_3, 2.16% Fe_2O_3, 2.29% CaO, 3.64% MgO, 0.27% Na_2O, 2.53% K_2O. Some physicochemical properties of the RB can be given as particle size <32 μm, pH 6.0–7.5, cation exchange capacity 0.35 mmol/g, point of zero charge (pH_{PZC}) about 6.8.

2.1.2. Preparation of MMB

Manganese chloride and sodium hydroxide were mainly used in the modification of Rb to enhance the adsorption capacity of RB. 20 g of RB were immersed in sufficient 2.0 M sodium hydroxide and temperature of the reaction mixture was maintained at 90 °C for 4 h. The RB was dispersed into 150 mL of 0.1 M $MnCl_2$ aqueous solution. 300 mL of 0.1 M NaOH aqueous solution was added slowly with a drop rate 1 mL/h. The titration was carried out under nitrogen flow throughout the procedure to minimize unexpected reactions, e.g. formation of carbonate salts. The obtained powder was rinsed with 0.01 M HCl aqueous solution to remove the excess $Mn(OH)_2$ precipitated on the outer surface of the clay and further washed with deionized water. The oxidation was performed in aqueous suspension system at room temperature. The $Mn(OH)_2$ intercalated compound prepared as above was dispersed in 50 mL of 1.5 M H_2O_2 basic solution and vigorously stirred. The color of the sample immediately turned from original light color to dark brown, indicating the oxidation of the hydroxide into oxide phase. For equilibrium, the suspension was further stirred for 24 h. The powder sample was washed with deionized water and dried at 60 °C [26].

2.2. Methods

2.2.1. Characterization procedures

The mineralogical compositions of the RB and MMB samples were determined from the X-ray diffraction (XRD) patterns of the products taken on a Rigaku 2000 automated diffractometer using Ni filtered Cu Kα radiation. XRD analysis of the bentonite was performed using the three-principal lines [27]. IR spectra of the bentonite samples were recorded in the region 4000–400 cm^{-1} on a Mattson-1000 FTIR spectrometer at 4 cm^{-1} resolution. A Tri Star 3000 (Micromeritics, USA) surface analyzer was used to measure nitrogen adsorption isotherm at 77 K in the range of relative pressure 10^{-6} to 1. Before measurement, the sample was degassed at 300 °C for 2 h. The surface areas were calculated by the BET (Brunauer–Emmett–Teller) method. The BET surface area (S_{BET}), external surface area (including only mesopores $S_{ext.}$), micropores surface area ($S_{mic.}$), total pore volume (V_t) and average pore diameter (D_p) results obtained by applying the BET equation to N_2 adsorption at 77 K and Barret–Joymer–Halenda (BJH) equation to N_2 adsorption at 77 K are listed in Table 1.

2.2.2. Cu(II) adsorption procedures

Adsorption experiments were carried out in polyethylene test tubes at 23 ± 2 °C by using the batch technique. The reaction mixture consisted of a total 50 mL containing 2 g/L adsorbent and the desired concentration of Cu(II) ions. All reagents used were of analytical grade. Cu(II) adsorption studies were followed as described by Sarkar et al. [28,29]. A solution of 1.0 mM Cu(II) was prepared from $Cu(NO_3)_2{\cdot}5H_2O$ by dissolving in deionised water. The stock was diluted to prepare a working solution of 0.5 mM Cu(II). The background electrolyte solutions

Table 1
Porous structure parameters of the RB and MMB samples

Sample	S_{BET} (m^2/g)	$S_{ext.}$[a]	$S_{mic.}$	V_t (cm^3/g)	$V_{mic.}$	$V_{meso.}$	D_p[b] (nm)
RB	36.17	19.86	16.30	0.07	0.008	0.067	8.11
MMB	63.70	36.80	26.90	0.08	0.013	0.067	5.30

[a] $S_{ext} = S_{meso.}$
[b] $4V/A$ by BET.

were 0.02, 0.05, and 0.1 M KNO_3. Solution pH was adjusted with 0.1 M HNO_3 or 0.1 M NaOH, such that the equilibrium solutions had pH values ranging from 3.0 to 6.5. Preliminary kinetic studies indicated that Cu(II) adsorption was characterized by a rapid initial adsorption (within 1 h) followed by a much slower, continuous uptake. A 24-h contacting period was found to be sufficient to achieve equilibrium. The separation of the liquid from the solid phase was achieved by centrifugation at 4500 rpm for 20 min. Adsorbed Cu(II) was calculated from the difference between the Cu(II) initially added to the system and that remaining in the solution after equilibration by a Unicam 929 model flame atomic absorption spectrophotometer. The dilutions induced by the pH controls were considered while computing the amount of Cu(II) adsorbed. Cu(II) adsorption in the presence of Cl^-, SO_4^{2-}, and HPO_4^{2-} was performed by equilibrating 0.05 g of bentonite in 20 mL of 0.25 M KNO_3 background electrolyte, 10 mL of Cu(II) working solution, and 20 mL of a NaCl, Na_2SO_4, or a Na_2HPO_4 working solution (achieving 0.01 M Cl^-, 0.01 M SO_4^{2-}, or 0.01 M HPO_4^{2-}) in 50-mL polyethylene test tubes. These experiments were performed in duplicate.

3. Results and discussion

3.1. Adsorbent characterization

3.1.1. XRD studies

The XRD patterns of RB and MMB samples were presented in Fig. 1. For the XRD pattern of RB, one reflection was observed in the region $2^\circ < 2\theta < 8^\circ$ (Fig. 1A). This corresponds to the 5.76 (2θ) value from which the interlamellar distance was found to be 15.33 Å. The position of d_{001} peak of MMB sample shifted from 15.33 to 12.41 Å (Fig. 1B). The formation of a new structure was illustrated by the peak appearing at 5.12° (2θ) in the XRD pattern of the MMB. This new peak situated at lower 2θ value was likely to appear because of agglomeration of the MMB sheets [30]. The XRD pattern of the MMB indicated that the MnO_2 saturation caused changing in unit cell dimensions.

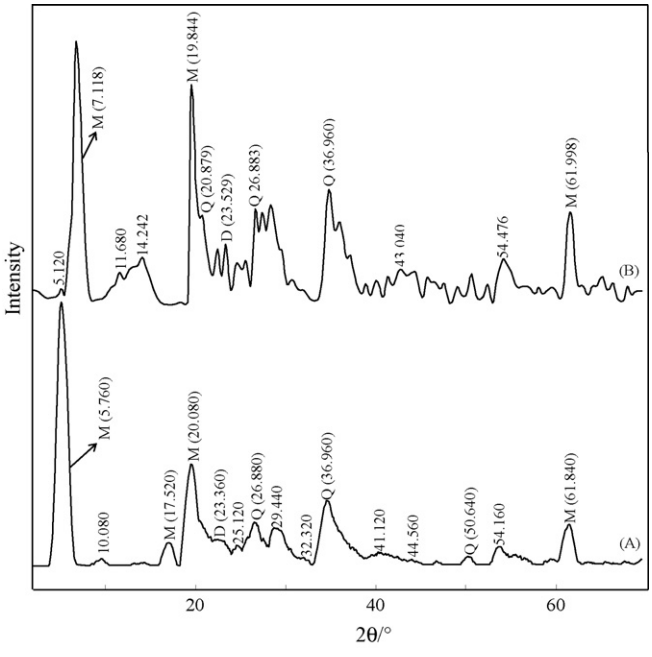

Fig. 1. The XRD patterns of the RB (A) and MMB (B) samples (M: montmorillonite, D: Dolomite, Q: quartz).

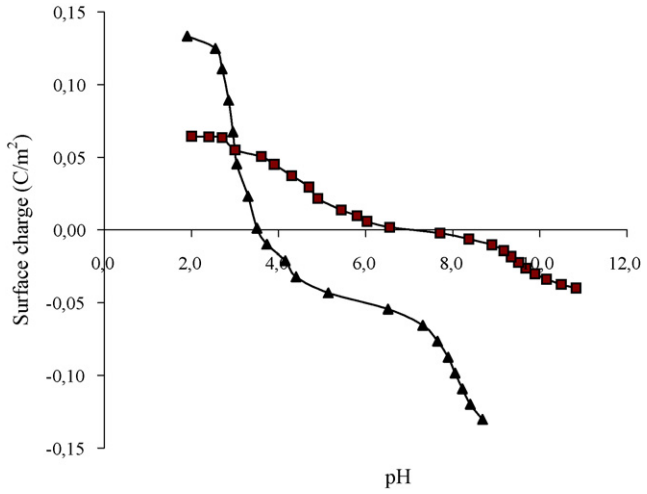

Fig. 2. Surface charge (C/m^2) vs. pH curves of bentonite samples in 0.1 M NaCl solution, squares, RB; triangles, MMB.

3.1.2. Proton adsorption studies

To better understand surface properties, potentiometric titrations were conducted. Fig. 2 shows proton adsorption curves performed at 0.1 M NaCl supporting electrolyte concentration for the RB and MMB samples. As shown in Fig. 2, the pH_{PZC} of RB is approximately 6.8. The MMB sample behaved similarly to MnO_2 where pH_{PZC} of MMB (3.5) is close to that of MnO_2 (2.4) [31]. The results suggest that the pH_{PZC} of MMB falls between the RB and MnO_2 and MnO_2-modification process plays important role in surface charge behavior of the adsorbent.

3.1.3. IR studies

Fig. 3a shows the infrared spectrum (IR) of the RB sample. The absorption band at 3635 cm^{-1} is due to stretching vibrations of structural OH groups of montmorillonite. The bands corresponding to AlAlOH, AlFeOH and AlMgOH bending vibrations were observed at 936, 885 and 845 cm^{-1}, respectively. A complex band at 1038 cm^{-1} is related to the stretching vibrations of Si–O groups, while the bands at 527 and 470 cm^{-1} are due to Al–O–Si and Si–O–Si bending vibrations, respectively. The band at 629 cm^{-1} was assigned to coupled Al–O and Si–O out-of-plane vibrations. The H_2O-stretching vibration was observed as a broad band at 3415 cm^{-1}. The shoulder near 3330 cm^{-1} is due to an overtone of the bending vibration of water observed at 1651 cm^{-1} [32]. Fig. 3b shows the IR spectrum of the MMB sample. Several absorption bands were observed at 3445, 1635, 1384, 1126, 577 and 535 cm^{-1}, respectively. The 3445 cm^{-1} band should be attributed to the O–H stretching vibration, and the 1625, 1348 bands are normally attributed to O–H bending vibrations combined with Mn atoms. The broad bands at 553 and 476 cm^{-1} should be ascribed to the Mn–O vibrations [32,33]. Detailed analysis of IR spectra in the whole spectral

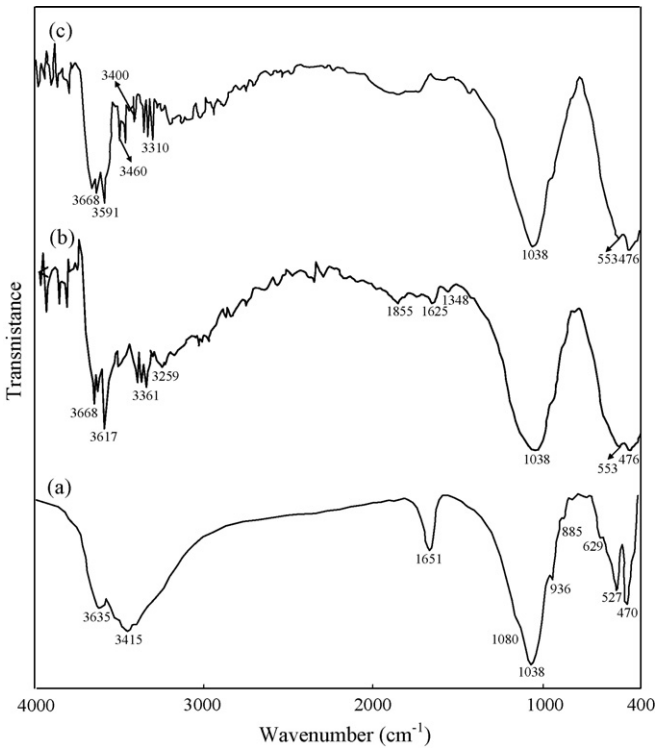

Fig. 3. IR spectra of the RB (a), MMB (b), and MMB–Cu(II) (c).

region (4000–400 cm^{-1}) can be used for discern of the location of Cu(II) cations [12,14]. The structural modifications of surface due to the adsorbed Cu(II) cations influence the fundamental vibrations of OH groups (Fig. 3c). For example, the stretching OH band was shifted up to 3668 cm^{-1} and, moreover, new bands appeared near 3591 and 3460 cm^{-1} in the spectrum of MMB–Cu(II) sample. The IR spectrum of the MMB–Cu(II) sample showed a strong band of water near 3400, due to the overlapping asymmetric ν_3 and symmetric ν_1 (H–O–H) stretching vibrations. The absorption band near 1635 cm^{-1} is due to the ν_2 (H–O–H) bending vibration. The band of MMB–Cu(II) at 3310 cm^{-1} may ascribe to an overtone ($2\nu_2$) of the bending mode [34]. The broad band near 1038 cm^{-1}, assigned to complex Si–O stretching vibrations in the tetrahedral sheet. The position of the Mn–O bond vibration at 553 cm^{-1} remained basically unchanged for the MMB–Cu(II) sample, but some broadening and a decrease in intensity of this band was observed.

3.2. Adsorption of Cu(II) by MMB sample

3.2.1. Adsorption model

The Langmuir and Freundlich isotherm models were applied to the experimental data (Figs. 4 and 5). The data conform the linear form of Langmuir model (Eq. (1)) [35] expressed below:

$$\frac{C_e}{q_e} = \frac{C_e}{q_m} + \frac{1}{K_L q_m} \quad (1)$$

where C_e is equilibrium concentration of Cu(II) (mg/L) and q_e is the amount of the Cu^{2+} adsorbed (mg) by per unit of bentonite (g). q_m and K_L are the Langmuir constants related to the

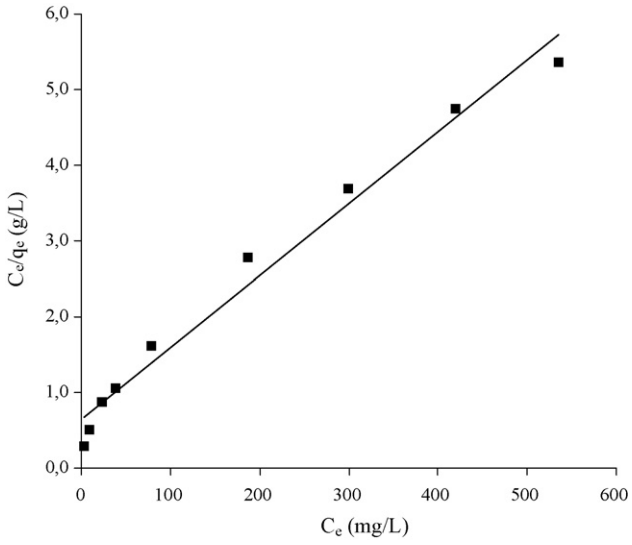

Fig. 4. Langmuir isotherm plot for the adsorption of Cu^{2+} onto the MMB sample. T = 295.15 K, initial pH 6.0, m = 2 g/L.

adsorption capacity (mg/g) and the equilibrium constant (L/g), respectively. The Langmuir monolayer adsorption capacity (q_m) gives the amount of the metal required to occupy all the available sites per unit mass of the sample. The Langmuir monolayer adsorption capacities of RB and MMB were estimated as 42.41 and 105.38 mg/g, respectively (Table 2). The value of maximum adsorption capacity (q_m) calculated from the Langmuir isotherm in this study is much higher than that of those reported in the literature. For example, adsorption of Cu(II) at 308 K on waste iron oxide follows the Langmuir isotherm model with an adsorption capacity of 14.10 mg/g [36]. Amarasinghe and William [37] have reported a Langmuir monolayer capacity, q_m, of 48 mg/g at for Cu(II) adsorption on tea waste. Langmuir adsorption capacity for Cu(II) adsorption on shells of lentil, wheat, and rice has been shown to be 8.97, 16.07 and 2.31 mg/g, respectively, by Aydın et al. [38]. The uptake of Cu(II) on spent activated clay has Lang-

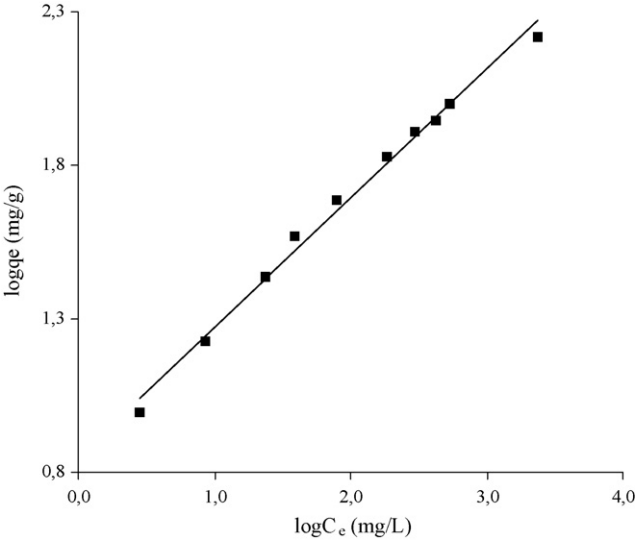

Fig. 5. Freundlich isotherm plot for adsorption of Cu^{2+} on the MMB sample. T = 295.15 K, initial pH 6.0, m = 2 g/L.

Table 2
Langmuir and Freundlich isotherm parameters for the adsorption of Cu^{2+} onto bentonite samples

Sample	Langmuir isotherm constants			Freundlich isotherm constants			D–R isotherm constants		
	q_m (mg/g)	K_L (L/g)	R^2	n	K_f	R^2	q_m (mg/g)	E (kJ/mol)	R^2
RB	42.41	0.20	0.992	2.38	8.77	0.990	6.55	0.75	0.842
MMB	105.38	0.08	0.980	2.28	6.69	0.994	12.16	2.24	0.969

muir monolayer capacity $q_m = 13.2$ mg/g at pH 6.0 [39]. Ok et al. [40] reported that the Langmuir adsorption capacity for Cu(II) on zeolite was found as 23.25 mg/g. As given in Table 2, the equilibrium constant K_{L1} (RB) value was much higher than K_{L2} (MMB). The high-energy sites with high equilibrium constant (K_{L1}) had a significantly lower affinity than that for low-energy sites with low equilibrium constant (K_{L2}). The high-energy sites on which Cu(II) was tightly held had a low adsorption maximum ($q_{m,1}$). The low energy sites on which Cu(II) were loosely held had a high adsorption maximum ($q_{m,2}$).

The adsorption equilibrium data was also applied to the Freundlich model (Eq. (2)) [41] given below:

$$\log q_e = \log K_f + \left(\frac{1}{n}\right) \log C_e \quad (2)$$

where K_f and n are Freundlich constants related to adsorption capacity and adsorption intensity, respectively. Freundlich parameters (K_F and n) indicate whether the nature of adsorption is either favorable or unfavorable. The intercept is an indicator of adsorption capacity and the slope is an indicator of adsorption intensity. A relatively slight slope $n \ll 1$ indicates that adsorption intensity is good (or favorable) over the entire range of concentrations studied, while a steep slope ($n > 1$) means that adsorption intensity is good (or favorable) at high concentrations but much less at lower concentrations. A high value of the intercept, K_F, is indicative of a high adsorption capacity. In the adsorption system, n value is 2.28 which indicates that adsorption intensity is good (or favorable) over the entire range of concentrations studied. The K_F value of the Freundlich equation (Table 2) also indicates that MMB has a very high adsorption capacity for copper ions in aqueous solutions.

The equilibrium data were also applied to the Dubinin–Radushkevich (D–R) isotherm model to determine if adsorption occurred by physical or chemical processes. The linearized form of the D–R isotherm [42–46] is as follows:

$$\ln q_e = \ln q_m - \beta\varepsilon^2 \quad (3)$$

where β is the activity coefficient related to mean adsorption energy (mol^2/J^2) and ε is the Polanyi potential ($\varepsilon = RT\ln(1 + (1/C_e))$). The D–R isotherm is applied to the data obtained from the empirical studies. A plot of $\ln q_e$ against ε^2 is given in Fig. 6. D–R isotherm constants, q_m, for RB and MMB were found to be 6.55 and 12.16 mg/g, respectively (Table 2). The difference of q_m derived from the Langmuir and D–R models is large. The difference may be attributed to the different definition of q_m in the two models. In Langmuir model, q_m represents the maximum adsorption of metal ions at monolayer coverage, whereas it represents the maximum adsorption of metal ions at the total specific micropore volume of the adsorbent in D–R model. Thereby, the value of q_m derived from Langmuir model is higher than that derived from D–R model. The differences are also reported in previous studies [42,44] (Fig. 7).

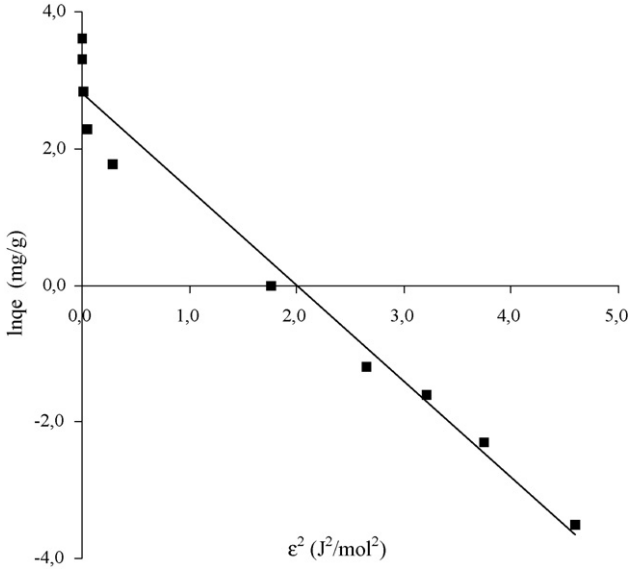

Fig. 6. D–R isotherm plot for adsorption of Cu^{2+} on the MMB sample. $T = 295.15$ K, initial pH 6.0, $m = 2$ g/L.

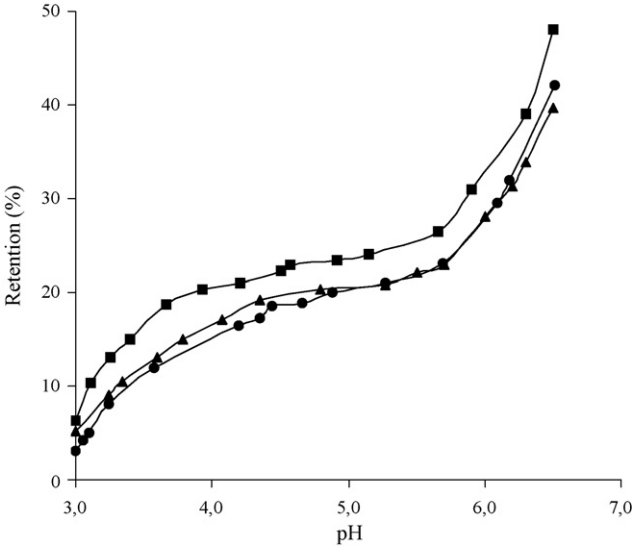

Fig. 7. Adsorption of Cu(II) (6.4 mg/L) by MMB (2 g/L) as function of pH and ionic strength (controlled by KNO_3), squares, 1.0 M; diamond-shaped, 0.1 M; triangles, 0.05 M; circles, 0.02 M.

The mean adsorption energy, E (kJ/mol) is as follows:

$$E = \frac{1}{\sqrt{-2\beta}} \quad (4)$$

This adsorption potential is independent of the temperature, but it varies depending on the nature of adsorbent and adsorbate. The magnitude of E is used for estimating the type of adsorption mechanism. If the E value is between 8 and 16 kJ/mol, the adsorption process follows by chemical adsorption and if $E < 8$ kJ/mol, the adsorption process is of a physical nature [42–46]. The calculated values of E are 0.75 and 2.24 kJ/mol for RB and MMB, respectively, and they are in the range of values for physical adsorption reactions. The similar results for the adsorption of Cr(III), Pb(II) and Zn(II) were reported by earlier workers [42,46].

The pH of the solution at the end of experiments was observed to be decreased after adsorption by MMB. This result indicated that the mechanism by means of which Cu(II) ion was adsorbed onto MMB perhaps involved an exchange reaction of Cu^{2+} with H^+ on the surface and surface complex formation. According to the principle of ion-exchange, the more metal ions is adsorbed onto MMB, the more hydrogen ions are released, thus the pH value was decreased. The hydrogen ion sources are most likely the hydroxyl groups in the MMB. Based on the above analysis, it is considered that the inner-sphere complexation model should be the dominating adsorption mechanism for Cu(II) onto the MMB.

The complex reactions of Cu^{2+} with MMB may be written as follows (S: MMB surface):

$$S\text{–}OH + Cu^{2+} \rightarrow (S\text{–}O\text{–}Cu)^+ + H^+ \quad (5)$$

$$S\text{–}O^- + Cu^{2+} \rightarrow (S\text{–}O\text{–}Cu)^+ \quad (6)$$

$$2(S\text{–}OH) + Cu^{2+} \rightarrow (S\text{–}O)_2Cu + 2H^+ \quad (7)$$

$$2(S\text{–}O^-) + Cu^{2+} \rightarrow (S\text{–}O)_2\text{–}Cu \quad (8)$$

$$S\text{–}OH + Cu^{2+} + H_2O \rightarrow S\text{–}OCuOH + 2H^+ \quad (9)$$

3.2.2. Effect of ionic strength and pH

The adsorption of Cu(II) onto the bentonite samples as a function of ionic strength and pH was shown in Fig. 6. The Cu(II) removal by MMB was observed over a range of initial pH values between 3 and 6.5. The percent of copper removal by MMB increases with increasing initial solution pH. The adsorption curves for MMB are characterized by two distinct adsorption edges. For example, in the presence of 0.1 M KNO_3, the first stage of adsorption edge commenced about 6% Cu(II) adsorption at pH ∼ 3.0 and ended at pH ∼ 4.5, at which about 22% of the total Cu(II) had been adsorbed. The second stage started at pH 4.9 and continued up to pH 6.5 where about 48% of the total Cu(II) was adsorbed. The influence of initial pH on Cu(II) removal may be explained as follows: in the acidic condition, both the adsorbent and the adsorbate are positively charged and therefore, the net interaction is that of electrostatic repulsion. Besides, the higher concentration of H^+ ions present in the reaction mixture competes with the positively charged Cu(II) ions for the surface adsorbing sites, resulting in a decrease in the removal of Cu(II). Effects of ionic strength showed a little effect on Cu(II) adsorption on the MMB. The effect of ionic strength on Cu(II) adsorption may be explained by the formation of inner-sphere complexes since K^+ in the background electrolyte could not compete with the Cu(II) adsorbed on the inner-sphere adsorption sites. Similar observations were made for Cu(II) adsorption on oxide surfaces [28,29]. The adsorption data tend to support an inner-sphere Cu(II) adsorption mechanism [28,29]. The effect of ionic strength of the medium provided little competition for Cu(II) adsorption by MMB but had strong effect on the adsorption of Cu(II) by smectite group clay minerals [15,47–50]. Cu(II) adsorption by these minerals was considered to be primarily due to coulombic attraction of the Cu(II) by permanent negative charges on the minerals. For this reason, Cu(II) adsorption by these minerals was strongly influenced by the ionic strength of solution. Because the presence of the permanent negative charges originates a net negative potential at the edges, they change their effective affinity of edge groups for cations when the ionic strength is changed [51]. Boonfueng et al. [31] showed that the manganese oxide coated montmorillonite resulted in a poorly crystalline oxide. For the manganese oxide coated montmorillonite, the overall surface properties of the system were consistent with its discrete oxide counterparts. The greater adsorption of the Cu(II) by the MMB was most likely due to the above mentioned differences in the adsorption mechanism of smectite group clay minerals and MMB.

3.2.3. Effect of inorganic ligands

The XRD patterns of end members of MMB–Cu(II)–ligand systems are shown in Fig. 8 and the details of the reflection positions and intensities are reported in Table 3. Several reflections were observed in the region $2^\circ < 2\theta < 20^\circ$ for the pattern of the MMB–Cu(II) system. One reflection situated at 7.12° (2θ) corresponds to the basal space of montmorillonite, the other reflections situated at a lower 2θ values are likely to appear because of the agglomeration of clay sheets [30,52]. This resulted in the formation of a porous structure with 18.09 Å. The position of basal spacing peak of binary MMB–Cu(II) system essentially remained the same and it was also accompanied by an intensity decrease from 100 to 24% (Table 3). This finding shows that the basic structure of MMB was changed during the Cu(II) adsorption. The XRD pattern of the ternary MMB–Cu(II)–Cl system shows poor crystallinity, broad and less intense peaks compared to the MMB. The intensity loses in MMB–Cu(II)–Cl system is approximately 1.07-fold lower than in the MMB material counterparts. The disappearence of the porous structure in the presence of Cl^- ligand may be explained by disaggregation of the clay lamellar packages by suspending them in water. In the presence of SO_4^{2-} and HPO_4^{2-} ligands, the porous structure of MMB, destroyed in the presence of Cl^- ligand, was reappeared, as shown by the shoulder appearing at a low 2θ value. However, d-spacing determined from the position of the shoulder is bigger than that of the MMB. The reappearance of the porous structure indicated that these ligands are responsible for agglomeration.

The adsorption of Cu(II) by the MMB sample was influenced by the presence of Cl^-, SO_4^{2-} and HPO_4^{2-} (Fig. 9). It is clear that aqueous speciation influences Cu(II) adsorption in the inor-

Table 3
d-Spacing and relative intensity for different MMB–Cu(II)–ligand systems

MMB													
d (Å)	44.13	17.24	12.40	4.47	3.77	3.58	3.22	3.12	2.89	2.55	2.16	1.68	1.49
I/I_0	2	2	100	95	14	5	8	12	2	46	5	5	34
MMB–Cu													
d (Å)	30.55	18.09	12.39	4.45	3.79	3.46	3.23	3.12	2.90	2.57	2.21	1.68	1.49
I/I_0	6	5	24	100	12	10	21	3	8	63	2	14	38
MMB–Cu–Cl													
d (Å)	25.66	–	12.40	4.47	3.79	3.46	3.24	3.14	2.91	2.56	2.16	1.68	1.49
I/I_0	2	–	60	100	14	11	14	11	3	49	7	6	29
MMB–Cu–SO_4													
d (Å)	41.86	20.43	12.26	4.47	3.78	3.45	3.22	3.12	2.89	2.53	2.20	1.68	1.49
I/I_0	2	2	77	100	20	12	39	28	5	41	8	12	39
MMB–Cu–PO_4													
d (Å)	42.44	21.22	12.40	4.48	3.79	3.47	3.22	3.16	2.90	2.56	2.23	1.69	1.49
I/I_0	10	9	43	100	18	11	16	8	8	61	6	12	37

ganic ligand systems. The adsorbed Cu(II) in the presence of inorganic ligands may be also attributed to a high specifity of the surfaces for Cu(II) relative to ligands. The percent Cu(II) adsorbed in the 0.01 M Cl^- systems at pH 6.0 are 33% for the MMB sample, compared to 39% at the same pH but in the absence of Cl^-. The decreased amount of adsorbed Cu(II) can be explained in terms of solution chemistry. Because, $CuCl^+$, $CuCl_2$, $CuCl_3^-$, $CuCl_4^{2-}$, CuOH–Cl and $Cu(OH)_2$ complexes are the dominate Cu(II) species in the presence of 0.01 M Cl^-. The chloride ion effectively decreases the degree of hydrolysis of Cu(II) ion by blocking some of the co-ordination positions. Also, the reduction in Cu(II) adsorption on the MMB sample in the presence 0.01 M Cl^- might be due to chloride ion competition with the various Cu(II) species for adsorption sites {e.g. [XOH^+–Cl^-]}. Fig. 9 also showed that the retention of Cu(II) by MMB surface was enhanced in the presence of other inorganic ligands (0.01 M SO_4^{3-} and HPO_4^{2-}). This result suggests that the observed Cu(II) adsorption behavior in the MMB suspensions is influenced by both aqueous speciation and surface ligand complexation of Cu(II) ions. The specifically adsorbed ligand enhances Cu(II) retention by the surface complexation of Cu(II).

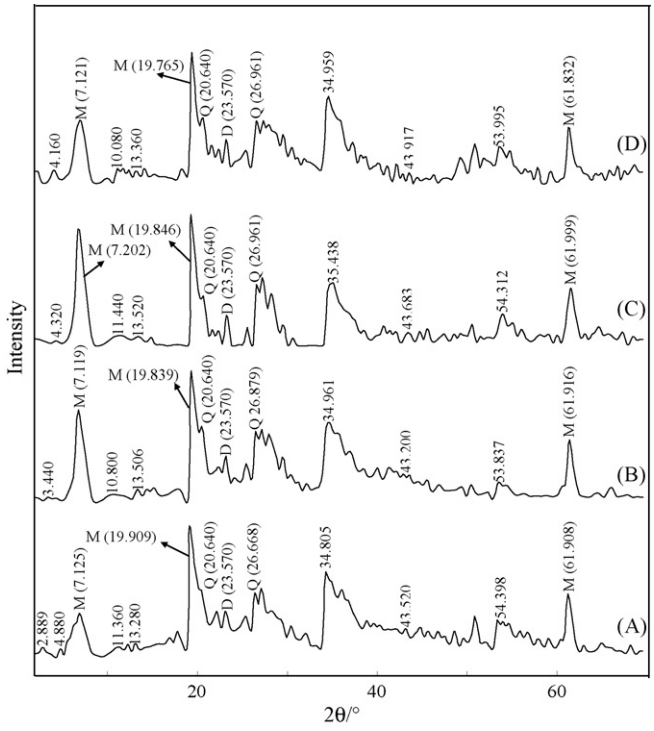

Fig. 8. The XRD patterns of the MMB–Cu(II) (A), MMB–Cu(II)–Cl (B), MMB–Cu(II)–SO_4 (C) and MMB–Cu(II)–HPO_4 (D) systems (M: montmorillonite, D: Dolomite, Q: quartz).

3.2.4. Thermodynamic studies

Using the following equations, the thermodynamic parameters of the adsorption process were determined from the experimental data:

$$\ln K_d = \frac{\Delta S}{R} - \frac{\Delta H}{RT} \quad (10)$$

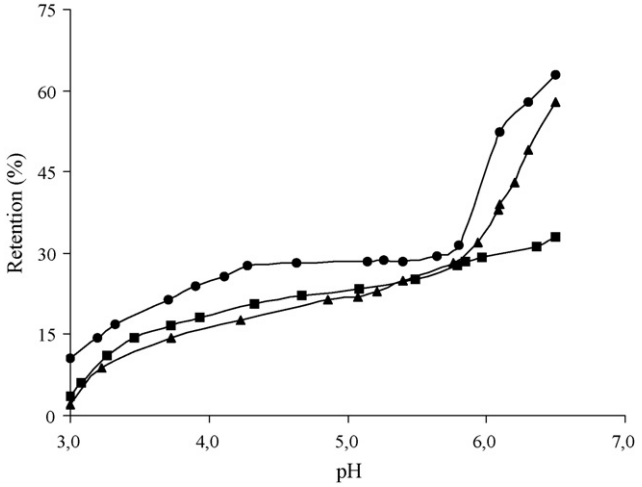

Fig. 9. Adsorption of Cu(II) (6.4 mg/L) by MMB (2 g/L) as function of pH and in the presence of Cl^-, SO_4^{2-}, and HPO_4^{2-} [ionic strength is 0.1 M (KNO_3); circles, HPO_4^{2-}; squares, SO_4^{2-}; triangles, Cl^-].

$$\Delta G = \Delta H - T\,\Delta S \quad (11)$$

$$K_d = \frac{q_e}{C_e} \quad (12)$$

where K_d is the distribution coefficient for the adsorption, ΔS, ΔH and ΔG are the changes of entropy, enthalpy and the Gibbs energy, T (K) is the temperature, R (J mol^{-1} K^{-1}) is the gas constant. The values of ΔH and ΔS were determined from the slopes and intercepts of the plots of ln K_d vs. $1/T$ (not showed).

The negative values for the Gibbs free energy change, ΔG, show that the adsorption process for the two bentonite samples is spontaneous and the degree of spontaneity of the reaction increases with increasing temperature. The increase in adsorption with temperature may be attributed to either increase in the number of active surface sites available for adsorption on the adsorbent or the desolvation of the adsorbing species and the decrease in the thickness of the boundary layer surrounding the adsorbent with temperature, so that the mass transfer resistance of adsorbate in the boundary layer decreases. The values of ΔG are less negative for the MMB suggesting that the adsorption process for this material is more spontaneous. These results suggest that the internal domains of this sample are more suitable environments for Cu(II) cations than the RB sample. The data shown in Table 4 show that the heats of adsorption are positive for both types of the bentonite samples. These positive values of ΔH indicate the endothermic behavior of the adsorption reaction of Cu(II) ions and suggest that a large amount of heat is consumed to transfer the Cu(II) ions from aqueous into the solid phase. As was suggested by Nunes and Airoldi [53], the transition metal ions must give up a larger share of their hydration water before they could enter the smaller cavities. Such a release of water from the divalent cations would result in positive values of ΔS. This mechanism of the adsorption of Cu(II) ions is also supported by the positive values of ΔS, which show that Cu(II) ions are less hydrated in the bentonite layers than in the aqueous solution. Also, the positive value of ΔS indicates the increased disorder in the system with changes in the hydration of the adsorbing Cu(II) cations.

3.2.5. Comparison of Cu(II) removal with different adsorbents reported in literature

The adsorption capacities of the adsorbents for the removal of Cu(II) have been compared with those of other adsorbents reported in literature and the values of adsorption capacities have been presented in Table 5. The values reported in the form of monolayer adsorption capacity. The experimental data of the present investigation are comparable with the reported values.

Table 4
Thermodynamic parameters for the adsorption of Cu(II) onto bentonite samples

Sample	ΔH (kJ/mol)	ΔS (J/mol K)	ΔG (kJ/mol)			R^2
			303.15	313.15	323.15	
RB	10.36	42.00	−0.34	−0.52	−0.71	0.997
MMB	1.79	21.34	−4.68	−4.89	−5.10	0.996

Table 5
Adsorption results of copper(II) ions from the literature by various adsorbents

Adsorbent	Adsorption capacity (mg/g)	Ref. No
Granular act. carbon (GAC)	60	[22]
Mn-GAC	86	[22]
Çankırı bentonite	44.84	[46]
Na-Bentonite	30	[54]
Ca-Bentonite	7.72	[54]
Montmorillonite	28.80	[55]
Organo-bentonite	56.55	[56]
Diatomite	27.55	[58]
Mn-diatomite	55.56	[58]
Birnessite	80	[59]
Bentonite (Unye)	42.41	In this study
MMB	105.38	In this study

Comparison of maximum experimental adsorption capacities of Cu(II) for manganese oxide modified adsorbents are also given in Table 5 [22,57]. Maximum adsorption capacity of Cu(II) for the manganese oxide modified modified samples was approximately 1.5–2 times higher than that of the raw material. The Cu(II) sorption capacities of diatomite and Mn–diatomite were determined as 27.55 and 55.56 mg/g, respectively [57]. In another study, Fan and Anderson [22] studied with Mn oxide coated granular activated carbon, for Cu(II) removal from aqueous solution. They reported that the granular activated carbon adsorbed Cu(II) with the adsorption capability of 60 mg/g. The capacity of the granular activated carbon increased to 86 mg/g. The obtained results show that MMB has a high Cu(II) adsorption capacity (105.38 mg/g) in comparison in other studies. The comparison of q_m value of MMB used in the present study with those obtained in the literature shows that MMB is more effective for this purpose. From these observations, it is appeared that the surface properties of raw bentonite could be improved upon modification of manganese oxide as previously reported by other researchers [18,19,22,57].

3.2.6. The mechanism of the adsorption of Cu(II)

Some recent studies have provided direct evidence about mechanism of cation adsorption on manganese oxides [59,60], performed adsorption experiences by contacting Zn^{2+} and manganese oxide suspensions in 0.1 M $NaNO_3$ solution [61]. EXAFS studies revealed the formation of Zn^{2+} inner-sphere surface complexes [61]. In addition to these proofs, other experimental evidences must be considered. They are follows: (1) The displacement of H^+ from the surface that was measured in this work and discussed in Section 3.1.2. It suggests that adsorption takes places with the release of H^+. (2) The increment of the amount of adsorbed Cu(II), as pH value rises. (3) The fact that the effect of ionic strength on Cu(II) adsorption may be explained by the formation of inner-sphere complexes since K^+ in the background electrolyte could not compete with the Cu(II) adsorbed on the inner-sphere adsorption sites. In view of the fact that pointed above, it is evident that manganese oxide modification enhanced the sorption of Cu(II) significantly. It may be explained by considering the coordinative environments of copper ions and surface hydroxyl groups in hydrated surfaces. Surface hydrox-

yls may be present as bridging and terminal groups and metal centers may be coordinated with two or more hydroxyls. These differing configurations will give rise to terminal hydroxyl of different acidity [62].

4. Conclusions

The adsorption of Cu(II) depend upon the nature of the adsorbent surface and the species distribution of Cu(II) in solution, which mainly depends on the pH of the system. It is clearly seen from the graph that the q_e increases at a slower rate with an increase in pH of the initial suspension from 3.0 to ≈5.0, and then increases considerably as the pH increases further. The plots have good linearity in both the cases (Freundlich plot, $R^2 = 0.994$, Langmuir plot, $R^2 = 0.980$) at 298 K. The values of the adsorption coefficients indicate the favorable nature of adsorption of Cu(II) on the MMB. From the values of Langmuir monolayer capacity, q_m, it is concluded that the treatment with manganese oxide does increase the number of adsorption sites to a large extent. It is evident that manganese oxide modification enhanced the sorption of Cu(II) significantly. This may be attributed to the increase in the surface area for the MMB as well as the resultant surface charge offered by the manganese oxides on the bentonite surface. The increased Cu(II) adsorption by MMB in the presence SO_4^{2-} and HPO_4^{2-} might be due to the bridging surface complexes.

Acknowledgement

I thank Assoc. Prof. Dr. Yunus Önal in determining porous structures of bentonite samples.

References

[1] S. Nogué, P. Sanz, P. Munné, E. Gadea, Copper contamination from domestic tap water with a descaler, Bull. World Health Organ., Genebra 78 (4) (2000).
[2] N. Das, R.K. Jana, Adsorption of some bivalent heavy metal ions from aqueous solutions by manganese nodule leached residues, J. Colloid Interface Sci. 293 (2006) 253–262.
[3] M. Doğan, Y. Özdemir, M. Alkan, Adsorption kinetics and mechanism of cationic methyl violet and methylene blue dyes onto sepiolite, Dyes Pigm. 75 (2007) 701–713.
[4] A.K. Bhattacharya, S.N. Mandal, S.K. Das, Adsorption of Zn(II) from aqueous solution by using different adsorbents, Chem. Eng. J. 123 (2006) 43–51.
[5] F.A. Banat, B. Al-Bashir, S. Al-Asheh, O. Hayajneh, Adsorption of phenol by bentonite, Environ. Pollut. 107 (2000) 391–398.
[6] U. Kumar, Agricultural products and by-products as a low cost adsorbent for heavy metal removal from water and wastewater: a review, Sci. Res. Essay 1 (2006) 33–37.
[7] P.F. Luckham, S. Rossi, The colloidal and rheological properties of bentonite suspensions, Adv. Colloid Interface Sci. 82 (1999) 43–92.
[8] A. Tabak, B. Afsin, S.F. Aygun, E. Koksal, Structural characteristics of organo-modified bentonites of different origin, J. Therm. Anal. Cal. 87 (2007) 375–381.
[9] O. Abollino, M. Aceto, M. Malandrino, C. Sarzanini, E. Mentasti, Adsorption of heavy metals on Na-montmorillonite. Effect of pH and organic substances, Water Res. 37 (2003) 1619–1627.
[10] E. Álvarez-Ayuso, A. García-Sánchez, Removal of heavy metals from waste waters by natural and Na-exchanged bentonites, Clays Clay Miner. 51 (2003) 475–480.
[11] J. Madejová, J. Bujdák, M. Janek, P. Komadel, Comparative FT-IR study of structural modifications during acid treatment of dioctahedral smectites and hectorite, Spectrochim. Acta A 54 (1998) 1397–1406.
[12] J. Madejová, B. Arvaiová, P. Komadel, FTIR spectroscopic characterization of thermally treated Cu^{2+}, Cd^{2+}, and Li^+ montmorillonites, Spectrochim. Acta A 55 (1999) 2467–2476.
[13] J. Madejová, M. Janek, P. Komadel, H.J. Herbert, H.C. Moog, FTIR analyses of water in MX-80 bentonite compacted from high salinary salt solution systems, Appl. Clay Sci. 20 (2002) 255–271.
[14] J. Madejová, H. Pálková, P. Komadel, Behaviour of Li^+ and Cu^{2+} in heated montmorillonite: evidence from far-, mid-, and near-IR regions, Vib. Spectrosc. 40 (2006) 80–88.
[15] E. Eren, B. Afsin, An investigation of Cu(II) adsorption by raw and acid-activated bentonite: a combined potentiometric, thermodynamic, XRD, IR, DTA study, J. Hazard. Mater. 151 (2008) 682–691.
[16] W.P. Gates, P. Komadel, J. Madejová, J. Bujdák, J.W. Stucki, R.J. Kirkpatrick, Electronic and structural properties of reduced-charge montmorillonites, Appl. Clay Sci. 16 (2000) 257–271.
[17] P. Komadel, J. Madejová, J.W. Stucki, Structural Fe(III) reduction in smectites, Appl. Clay Sci. 34 (2006) 88–94.
[18] R. Han, W. Zou, H. Li, Y. Li, J. Shi, Copper(II) and lead(II) removal from aqueous solution in fixed-bed columns by manganese oxide coated zeolite, J. Hazard. Mater. 137 (2006) 934–942.
[19] R. Han, W. Zou, Z. Zhang, J. Shi, J. Yang, Removal of copper(II) and lead(II) from aqueous solution by manganese oxide coated sand: I. Characterization and kinetic study, J. Hazard. Mater. 137 (2006) 384–395.
[20] M. Nachtegaal, D.L. Sparks, Effect of iron oxide coatings on zinc sorption mechanisms at the clay-mineral/water interface, J. Colloid Interface Sci. 276 (2004) 13–23.
[21] L.C.A. Oliveira, R.V.R.A. Rios, J.D. Fabris, K. Sapag, V.K. Garg, R.M. Lago, Clay–iron oxide magnetic composites for the adsorption of contaminants in water, Appl. Clay Sci. 22 (2003) 169–177.
[22] H.-J. Fan, P.R. Anderson, Copper and cadmium removal by Mn oxide-coated granular activated carbon, Sep. Purif. Technol. 45 (2005) 61–67.
[23] Y. Xu, T. Boonfueng, L. Axe, S. Maeng, T. Tyson, Surface complexation of Pb(II) on amorphous iron oxide and manganese oxide: spectroscopic and time studies, J. Colloid Interface Sci. 299 (2006) 28–40.
[24] S.S. Tripathy, S.B. Kanungo, Adsorption of Co^{2+}, Ni^{2+}, Cu^{2+} and Zn^{2+} from 0.5 M NaCl and major ion sea water on a mixture of δ–MnO_2 and amorphous FeOOH, J. Colloid Interface Sci. 284 (2005) 30–38.
[25] H. Tamura, N. Katayama, R. Furuichi, The Co^{2+} adsorption properties of Al_2O_3, Fe_2O_3, Fe_3O_4, TiO_2, and MnO_2 evaluated by modeling with the Frumkin isotherm, J. Colloid Interface Sci. 195 (1997) 192–202.
[26] K. Fuda, S. Narita, Synthesis of layered transition metal oxide/clay nanocomposites., J. Ceram. Soc. Japan (Spec. Issue) 112 (2004) 717–723.
[27] R.W. Grimshaw, The Chemistry and Physics of Clays, Ernest Benn Ltd., London, 1971, pp. 968–979.
[28] D. Sarkar, M.E. Essington, K.C. Misra, Adsorption of mercury(II) by variable charge surfaces of quartz and gibbsite, J. Am. Soil Sci. Soc. 63 (1999) 1626–1636.
[29] D. Sarkar, M.E. Essington, K.C. Misra, Adsorption of mercury(II) by kaolinite, J. Am. Soil Sci. Soc. 64 (2000) 1968–1975.
[30] G. Szöllösi, A. Mastalir, M. Bartok, Effect of ion exchange by an organic cation on platinum immobilization on clays, React. Kinet. Catal. Lett. 74 (2001) 241–249.
[31] T. Boonfueng, L. Axe, Y. Xu, Properties and structure of manganese oxide-coated clay, J. Colloid Interface Sci. 281 (2005) 80–92.
[32] J. Madejová, FTIR techniques in clay mineral studies, Vib. Spectrosc. 31 (2003) 1–10;
T. Kohler, T. Armbruster, E. Libowitzky, Hydrogen bonding and Jahn–Teller distortion in groutite,α-MnOOH, and Manganite, γ-MnOOH, and their relations to the manganese dioxides Ramsdellite and Pyrolusite dioxides, J. Solid State Chem. 133 (1997) 486–500.
[33] K.M. Parida, S. Mallick, B.K. Mohapatra, V.N. Misra, Studies on manganese-nodule leached residues: 1. Physicochemical characterization

and its adsorption behavior toward Ni^{2+} in aqueous system, J. Colloid Interface Sci. 277 (2004) 48–54.
[34] J.L. Bishop, C.M. Pieters, J.O. Edwards, Infrared spectroscopic analyses on the nature of water in montmorillonite, Clays Clay Miner. 42 (1994) 702–716.
[35] I. Langmuir, The adsorption of gases on plane surfaces of glass, mica and platinum, J. Am. Soc. 40 (1918) 1361–1403.
[36] Y.-H. Huang, C.-L. Hsueh, H.-P. Cheng, L.-C. Su, C.-Y. Chen, Thermodynamics and kinetics of adsorption of Cu(II) onto waste iron oxide, J. Hazard. Mater. 144 (2007) 406–411.
[37] B.M.W.P.K. Amarasinghe, R.A. Williams, Tea waste as a low cost adsorbent for the removal of Cu and Pb from wastewater, Chem. Eng. J. 132 (2007) 299–309.
[38] H. Aydın, Y. Bulut, Ç. Yerlikaya, Removal of copper (II) from aqueous solution by adsorption onto low-cost adsorbents, J. Environ. Manage. 87 (2008) 37–45.
[39] C.-H. Weng, C.-Z. Tsai, S.-H. Chu, Y.C. Sharma, Adsorption characteristics of copper(II) onto spent activated clay, Sep. Purif. Technol. 54 (2007) 187–197.
[40] Y.S. Ok, J.E. Yang, Y.-S. Zhang, S.-J. Kim, D.-Y. Chung, Heavy metal adsorption by a formulated zeolite–Portland cement mixture, J. Hazard. Mater. 147 (2007) 91–96.
[41] H. Freundlich, Über die adsorption in lösungen, Zeitschrift für Physikalische Chemie (Leipzig) 57 (1906) 385–470.
[42] A. Sarı, M. Tuzen, M. Soylak, Adsorption of Pb(II) and Cr(III) from aqueous solution on Celtek clay, J. Hazard. Mater. 144 (2007) 41–46.
[43] A. Sarı, M. Tuzen, D. Cıtak, M. Soylak, Adsorption characteristics of Cu(II) and Pb(II) onto expanded perlite from aqueous solution, J. Hazard. Mater. 148 (2007) 387–394.
[44] D. Xu, X.L. Tan, C.L. Chen, X.K. Wang, Adsorption of Pb(II) from aqueous solution to MX-80 bentonite: effect of pH, ionic strength, foreign ions and temperature, Appl. Clay Sci. 41 (2008) 37–46.
[45] A. Günay, E. Arslankaya, İ. Tosun, Lead removal from aqueous solution by natural and pretreated clinoptilolite: adsorption equilibrium and kinetics, J. Hazard. Mater. 146 (2007) 362–371.
[46] S. Veli, B. Alyüz, Adsorption of copper and zinc from aqueous solutions by using natural clay, J. Hazard. Mater. 149 (2007) 226–233.
[47] S.J. Traina, H.E. Doner, Co, Cu, Ni, and Ca sorption by a mixed suspension of smectite and hydrous manganese dioxide, Clays Clay Miner. 33 (1985) 118–122.
[48] L.I. Vico, Acid–base behaviour and Cu^{2+} and Zn^{2+} complexation properties of the sepiolite/water interface, Chem. Geol. 198 (2003) 213–222.
[49] D.E. Egirani, A.R. Baker, J.E. Andrews, Copper and zinc removal from aqueous solution by mixed mineral systems: I. Reactivity and removal kinetics, J. Colloid Interface Sci. 291 (2005) 319–325.
[50] D.E. Egirani, A.R. Baker, J.E. Andrews, Copper and zinc removal from aqueous solution by mixed mineral systems: II. The role of solution composition and aging, J. Colloid Interface Sci. 291 (2005) 326–333.
[51] M.J. Avena, M.M. Mariscal, C.P. De Pauli, Proton binding at clay surfaces in water, Appl. Clay Sci. 24 (2003) 3–9.
[52] D. Dermatas, M.S. Dadachov, Rietveld quantification of montmorillonites in lead-contaminated soils, Appl. Clay Sci. 23 (2003) 245–255.
[53] L.M. Nunes, C. Airoldi, Some features of crystalline α-titanium hydrogenphosphate, modified sodium and *n*-butylammonium forms and thermodynamics of ionic exchange with K^+ and Ca^{2+}, Thermochim. Acta 328 (1999) 297–305.
[54] E. Alvarez-Ayuso, A. Garcia-Sanchez, Removal of heavy metals from waste waters by natural and Na-exchanged bentonites, Clay Miner. 51 (2003) 475–480.
[55] K.G. Bhattacharyya, S.S. Gupta, Kaolinite, montmorillonite, and their modified derivatives as adsorbents for removal of Cu(II) from aqueous solution, Sep. Purif. Technol. 50 (2006) 388–397.
[56] Ö. Gök, A. Özcan, B. Erdem, A.S. Özcan, Prediction of the kinetics, equilibrium and thermodynamic parameters of adsorption of copper(II) ions onto 8-hydroxy quinoline immobilized bentonite, Colloids Surf. A Physicochem. Eng. Asp. 317 (2008) 174–185.
[57] M.A.M. Khraisheh, Y.S. Al-Degs, W.A.M. Mcminn, Remediation of wastewater containing heavy metals using raw and modified diatomite, Chem. Eng. J. 99 (2004) 177–184.
[58] X.H. Feng, L.M. Zhai, W.F. Tan, F. Liu, J.Z. He, Adsorption and redox reactions of heavy metals on synthesized Mn oxide minerals, Environ. Pollut. 147 (2007) 366–373.
[59] C.L. Peacock, D.M. Sherman, Sorption of Ni by birnessite: Equilibrium controls on Ni in seawater, Chem. Geol. 238 (2007) 94–106.
[60] B. Lanson, V.A. Drits, A.-C. Gaillot, E. Silvester, A. Plançon, A. Manceau, Structure of heavy-metal sorbed birnessite: Part 1. Results from X-ray diffraction, Am. Miner. 87 (2002) 1631–1645.
[61] X. Li, G. Pan, Y. Qin, T. Hu, Z. Wu, Y. Xie, EXAFS studies on adsorption–desorption reversibility at manganese oxide–water interfaces: II. Reversible adsorption of zinc on δ-MnO_2, J. Colloid Interf. Sci. 271 (2004) 35–40.
[62] P.J. Pretorius, P.W. Linder, The adsorption characteristics of δ-manganese dioxide: a collection of diffuse double layer constants for the adsorption of H^+, Cu^{2+}, Ni^{2+}, Zn^{2+}, Cd^{2+} and Pb^{2+}, Appl. Geochem. 16 (2001) 1067–1082.